Journal of Statistical Physics, Vol. 51, Nos. 5/6, 1988

Micro-Hydrodynamics

L. Hannon,[1,2] G. C. Lie,[1] and E. Clementi[1]

Received February *24, 1988*

Micro-hydrodynamics is a term used to describe the search for and study of hydrodynamic phenomena at microscopic scales. The principal method used to accomplish this research is molecular dynamic (MD) simulations. Computational limits on MD models restrict the size of the system and simulation time. Typically, the length scales are on the order of 10–1000 Å and time scales 10–1000 psec (thus the qualifier micro). We review the results of our research in this area. We use MD to model channel flow, flow past a plate, flow past a cylinder, and Rayleigh–Benard convection. In general, we find that the behavior in these models agrees with results obtained from experiment and more traditional theoretical approaches, such as solving the Navier–Stokes equations. In addition to the appearance of spatial and temporal patterns, we observe scaling relations in agreement with those predicted by macroscopic hydrodynamics. In some specific situations, we can see the breakdown of Navier–Stokes theory and estimate its limits.

KEY WORDS: Molecular dynamics simulation; hydrodynamics.

1. INTRODUCTION

Molecular dynamics (MD) simulations have been used over the past 30 years to study behavior in a large variety of systems. It has proved to be a valuable tool for research of behavior in gases, liquids, and solids both in and out of equilibrium. The facets of behavior studied are far too numerous to mention. Instead, we will concentrate on the study of dynamical behavior in fluids and refer the interested reader to several excellent review articles.[1–3]

As recently as 2 years ago, the study of nonequilibrium fluids covered only the very simple situations where the system is subjected to either a thermal gradient[4–7] or a constant shear.[8–14] These two systems are

[1] Department 48B/MS 428, Data Systems Division, IBM Corporation, Kingston, New York 12401.

[2] Present address: Department 63G/MS 36, IBM Corporation, Palo Alto, California 94304.

0022-4715/88/0600-0965$06.00/0 © 1988 Plenum Publishing Corporation

important in studying the behavior of transport coefficients as a function of the applied gradient. It was observed in these simulations that such systems obey Poisson's equation even when the gradients are extremely large (up to 10^9 K/cm for the thermal gradient and 10^{10} cm/sec for the velocity gradient). That is, the resulting behavior agreed with that predicted by macroscopic theory. However, at this time, the question still remained as to whether simulations of systems of particles moving along trajectories governed by Newton's laws of motion could exhibit the spatial and/or temporal structures seen in experimental and theoretical studies of macroscopic systems. An even more important question is, given that these structures can be seen at microscopic scales, would they behave according to the scaling relations observed in macroscopic fluid dynamics?

The initial objective of our research was therefore to determine if such structures could be seen in MD simulations. As the research progressed, we found that the answer to the above two questions is affirmative. The initial objective thus evolved into three objectives, all of which are currently under investigation. First, to determine the kinds of hydrodynamic behavior that can be observed in MD simulations. Second, to develop the relationship between microscopic and macroscopic behavior. And, finally, to provide information on phenomena that can only be studied from a microscopic point of view due to inherent limits of Navier–Stokes theory.

The computational facilities at the IBM Scientific and Engineering Center in Kingston, New York allow simulations of systems of up to 500,000 particles to be accomplished in a reasonable amount of time. Such large numbers are required to reach the critical values of the scaling numbers where bifurcations are expected to occur and to obtain a reasonable signal-to-noise ratio in cells representing the smallest scales over which measurements are taken. The LCAP-2 computer is comprised of ten FPS-264 processors with 1 megaword of local memory each attached to an IBM mainframe. The ten attached processors can be run in parallel. Interprocessor communications are accomplished through use of FPS buses or a separate bulk memory accessible to all processors. This facility allowed us to simulate 1 psec of system time (100 integrations of the 1,500,000 equations of motion) in as little as 3 min of real time.

2. THE MD MODEL

The MD model is a system of N particles enclosed in a parallelepiped of size $L_x \times L_y \times L_z$ (simulations of two-dimensional systems have $L_z = 1$). The atoms interact through a Lennard-Jones-type potential of the form

$$U(r) = 4\varepsilon \left[\left(\frac{\sigma}{r} \right)^{12} - \left(\frac{\sigma}{r} \right)^{6} + \frac{1}{4} \right] \tag{1}$$

with a range extending up to $2^{1/6}\sigma$. The short cutoff serves to speed up the computations without dramatically affecting the transport properties of the system. The parameters used for this potential function in our simulations correspond to the interatomic potential for argon, i.e., $\sigma = 3.405$ Å and $\varepsilon = 119.8k_B$. The average system density and temperature are chosen to reflect argon in the liquid state ($\rho = 0.845/\sigma^3$ in 3D, $\rho = 0.832/\sigma^2$ in 2D, and $T = 86.5$ K).

The system boundaries are variations of three basic types. Periodic boundaries are boundaries outside of which the system repeats itself. For example, in a system with periodic boundaries at $x = -L/2$ and $x = +L/2$, a particle located at $(0, y, z)$ will have images located at $(-L, y, z)$ and $(+L, y, z)$. Particles just inside the boundary at $x = +L/2$ will interact with images of particles just inside the boundary at $x = -L/2$; particles crossing the boundary at $x = +L/2$ will have images crossing the boundary at $x = -L/2$.

Thermal boundaries serve as a model for particle behavior at physical boundary walls. A particle colliding with a thermal boundary will be re-injected into the system with a new set of velocities drawn randomly from a Maxwell–Boltzmann distribution characterized by the wall temperature T_w. Since the components of the velocity in the directions parallel to the wall will, on average, vanish, thermal boundaries are considered to be models of no-slip boundaries. Specular boundaries, on the other hand, maintain continuity of the tangential components of velocity during a particle–wall interaction. These are then considered to be a model for slip boundaries. Particles located in the neighborhood of a specular boundary will experience a force directed along the shortest particle–wall distance of the same magnitude as the force exerted by a particle located just outside of the wall. In addition to the external boundary link to the outside world, the system can also be subject to acceleration fields of varying magnitude, which serve to induce a net flow.

The initial conditions for the system have the particles located on a cubic lattice with velocities drawn randomly from a Maxwell–Boltzmann distribution at $T = 86.5$ K. Interparticle forces are computed using a nearest neighbor cell search that minimizes the time spent searching for and eliminating particle pairs whose separation is greater than the potential cutoff. A fourth-order Adams–Bashforth predictor–corrector integrator is used to advance the particles along their trajectories.[15] The integration time step is dependent on the highest temperature achieved in the system. The condition that total energy be conserved in an equilibrium system at this temperature yields time steps in the 10^{-14} sec range. After each integration step, the particle–wall interactions are computed and the dynamics of the affected particles modified. The algorithm consists of the repetition of the steps: calculate the force on each particle, integrate the

equations of motion, and modify particle behavior to reflect boundary conditions.

For the purpose of measuring system behavior, the system is covered with a grid of cells. The values of the thermodynamic variables and their fluxes are computed for each cell by averaging the appropriate properties of the particles located inside the cell. The system is considered to be in its final state when its hydrodynamic variables (ρ, T, and v) measured at various points in the system are either stationary or exhibit steady oscillations over time.

3. CHANNEL FLOW

Channel flow is the two-dimensional analog of a pipe flow. Such a system describes behavior near the surface of a fluid flowing in a deep channel. In the MD model for channel flow,[16] we consider a system of particles bounded by thermal walls in one coordinate (say x) and periodic in the other coordinates (say y and/or z). Flow is induced by subjecting the particles to an acceleration field along a direction parallel to the thermal walls. A steady state will be reached when the energy added to the system from the acceleration field is balanced by the energy removed from the system through the thermal walls.

In this situation and assuming the fluid to be incompressible, the hydrodynamic equations for velocity and temperature reduce to

$$\nabla^2 \mathbf{v} = \frac{\rho \mathbf{g}}{\eta}$$

$$\nabla^2 T = -\frac{\eta}{2k} \sum_{i,j} \left(\frac{\partial v_i}{\partial x_j} + \frac{\partial v_j}{\partial x_i} \right)^2, \qquad ij = 1, 2, 3$$

where ρ is the mass density, g is the gravitational field, η is the dynamic viscosity, and k is the thermal conductivity.

When subjected to the boundary conditions

$$v_y(x = -L/2) = v_y(x = +L/2) = 0$$

and

$$T(x = -L/2) = T(x = +L/2) = T_w$$

these equations can be solved exactly, giving

$$v_y = \frac{\rho g}{2\eta} \left[x^2 - \left(\frac{L}{2} \right)^2 \right]$$

$$v_x = v_z = 0$$

$$T = T_w - \frac{1}{12} \frac{(\rho g)^2}{k\eta} \left[x^4 - \left(\frac{L}{2} \right)^4 \right]$$

Macroscopic theory predicts that the velocity will exhibit a parabolic profile and the temperature a quartic profile across the channel. Further, the viscosity and the thermal conductivity can be found from the curvatures of these profiles.

We have performed simulations for a large number of channel flow systems in which we studied behavior in two and three dimensions for a number of different channel widths and acceleration field magnitudes (initial results are contained in ref. 16). In all of these simulations, the expected behavior is observed. Away from the thermal walls, we see a parabolic profile for the velocity and a quartic profile for the temperature. Measurements of the profile curvatures yield viscosities and thermal conductivities that are consistent with values measured experimentally. In Fig. 1, we show the velocity and temperature as a function of the cross channel coordinate. Points reflect actual measurements taken from the steady-state MD simulation; lines reflect a least squares fit of the points to the expected form of the profile.

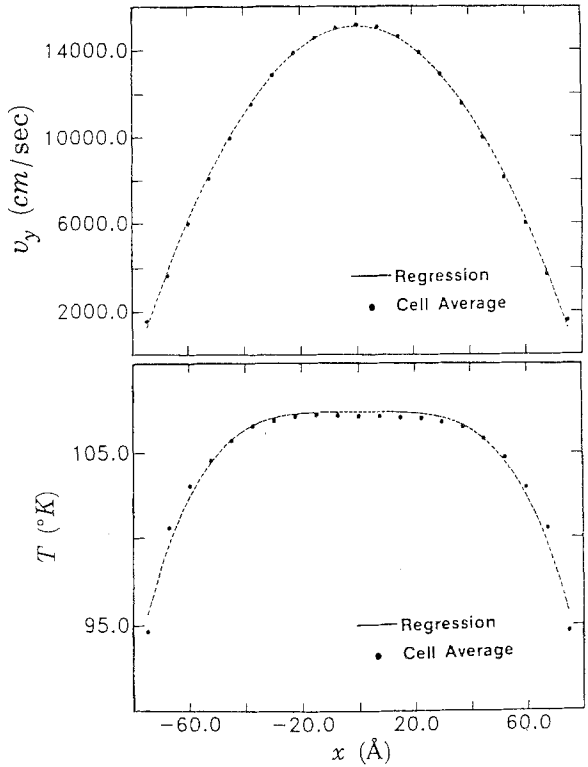

Fig. 1. Velocity (top) and temperature (bottom) profiles for a channel flow. The system consists of 21,000(42 × 500) atoms enclosed in a rectangular of 156.7 Å × 1866 Å.

In Fig. 2, we show the density as a function of the cross channel coordinate. The density is flat across the channel except in the regions close to the walls, where it seems to exhibit a sharp increase. Further simulations with a finer measurement grid give us a better idea of the actual behavior near the channel walls. The fluid organizes into a layer structure (see Fig. 2) within ten atomic diameters of the thermal walls. In our simulations, this layering phenomenon is independent of the magnitude of the acceleration field and the channel width. The layering has also been observed in other MD simulations where different potential functions and different models for the system boundaries are used.[17] The layering

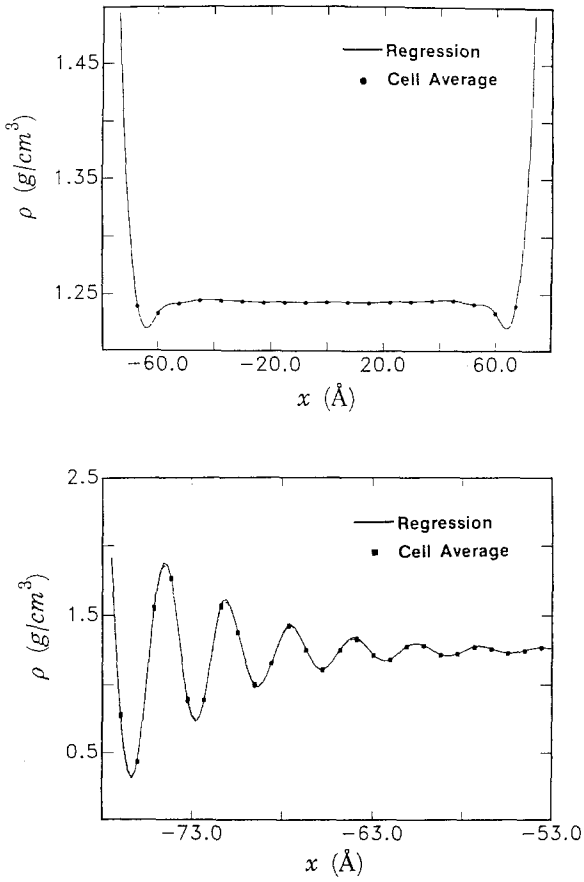

Fig. 2. Coarse-grid (top) and fine-grid (bottom) density profiles for the channel flow discussed in Fig. 1.

structure leads us to conclude that we are observing the breakdown of Navier–Stokes theory. There is some recent experimental evidence of this layering phenomena.[19]

4. FLOW PAST A PLATE

Fluid flowing past a flat plate should be the easiest system in which to observe spatial structure since, macroscopically, the system is expected to exhibit vortices at any nonzero Reynolds number[20] defined in this case to be

$$\mathrm{Re} = vL/v$$

where v is the velocity far from the plate, L is the plate length, and v is the kinematic viscosity. In fact, MD simulations of this system were the first such simulations to show the formation of spatial structures. Computer simulations have been performed for the situation where the plate is dragged through the fluid[21] and for the situation where the fluid is caused to flow past a stationary plate.[22] Our simulations involved the latter.

The MD system in this case consists of 10,000 particles in a rectangle (2D). The particles are caused to flow past a thermalizing plate by imposing an acceleration field in the direction normal to the plate. The boundaries parallel to the direction of flow are periodic. The boundaries at the head end and tail end of the flow are modified boundaries. These boundaries are separated by an equilibration region which behaves as a thermal bath. The computation of interparticle forces treats these boundaries as periodic. The computation of particle–wall interactions treats particles in the bath as if they were surrounded by thermal walls. Particles leaving the system must travel through the bath before they can be considered as candidates for reentry. During this time, the particles thermalize through interactions with the bath walls and other particles in the bath. Coincident with a particle entering the bath from the tail end of the system, the particle in the bath closest to the head end of the system is released for reentry. This device serves to separate behavior at the head end of the flow from that at the tail, keep a constant number of particles in the flow system, and maintain continuity of the interparticle potential.

The simulations were carried out for several values of the acceleration field strength: 0.625, 2.5, 5.0, and 10×10^{14} cm/sec^2. For system with $g = 2.5 \times 10^{14}$ cm/sec^2, the appearance of two counterrotating vortices immediately behind the obstructing plate is first observed after 120 psec of simulation time ($\langle v_x \rangle = 19{,}000$ cm/sec). The distance between the plate and the center of these vortices increases with increasing velocity until

the system reaches a steady state after 200 psec of simulation time ($\langle v_x \rangle = 21{,}500$ cm/sec). The vortex size and location, as well as the average system velocity, remain stable over an additional 300 psec of simulation time. The density contour and velocity field for the steady-state system based on statistics taken over the last 100 psec of simulation time are shown, respectively, in Fig. 3. Note that we take advantage of the symmetry about the midplane to enhance the signal and thus show only half of the system in the figure.

The small size of the system places inherent limitations on the range of parameters that can be simulated. For $g < 0.625 \times 10^{14}$ cm/sec^2, observation of the vortices is hindered by thermal noise (the average system velocity is

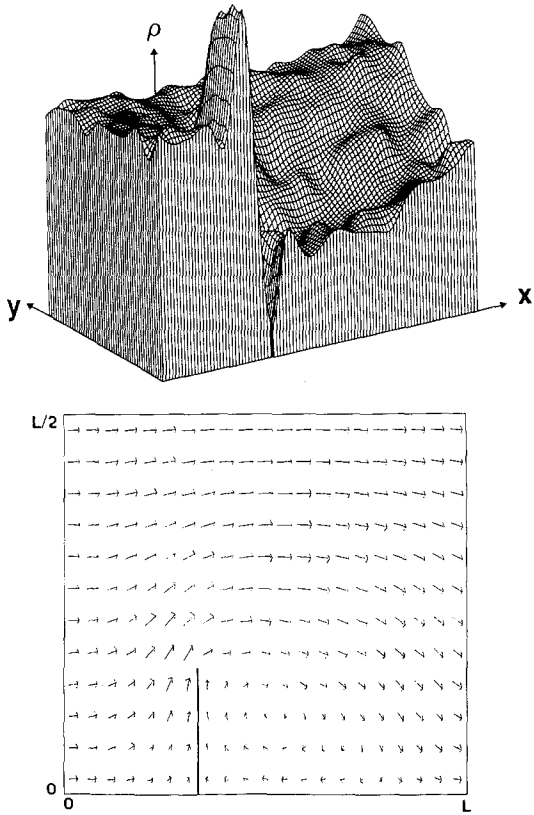

Fig. 3. Density contour (top) and velocity field (bottom) for a flow past a plate. The system consists of 10,000 particles in a square of side 373.22 Å. In the density contour, the baseline density is 1.125 g/cm^3. In the velocity field, the arrow lengths are scaled as the square root of the ratio of individual cell velocity to maximum cell velocity; the cell centers are located at the origins of the arrows.

of the order of thermal noise); for $g > 5 \times 10^{14}$ cm/sec^2, the vortex size is influenced by the presence of a boundary at $x = L$. In the range of velocities studied (0.135c to 0.480c, where c is the sound speed for argon at its triple point, 86,400 cm/sec), the fluid is highly compressible: densities in the system are found to range from 1.422 g/cm^3 immediately in front of the plate to 1.135 g/cm^3 immediately behind the plate for the system shown in Fig. 2. This large variation of the density and stress prevents us from making any realistic determination of the Reynolds number and thus making any quantitative comparisons with macroscopic theory. Nevertheless, within the above range of simulation parameters, we do observe that the vortex size and the steady-state distance between the plate and the vortex center are roughly proportional to the average mass flux in the system (which itself is proportional to the Reynolds number). This result is at least in qualitative agreement with the macroscopic theory.

5. FLOW PAST A CYLINDER

Encouraged by the results of the channel flow and flow past a plate, we have carried out a more thorough study of the flow past a cylinder. The behavior in this system can be characterized by two dimensionless scaling numbers.[23] The Reynolds number

$$\mathrm{Re} = 2vR/v$$

where R is the cylinder radius, can be considered a scaled velocity. The Strouhal number,

$$\mathrm{St} = 2R/v\tau$$

is a scaled time for temporal behavior in the system (τ is the characteristic time). Macroscopic experiments involving fluid flowing past a cylinder exhibit the formation of two counterrotating eddies immediately behind the cylinder at Reynolds numbers above 10. Periodic vortex shedding sets in at Reynolds number above 40 characterized by a Strouhal number starting at 0.11 and increasing with increasing Reynolds number to a maximum of about 0.22.[24] In an MD simulation of this system we should be able to observe the periodic behavior. In addition, this will give us a chance to compare microscopic values of the scaling numbers with macroscopic observations.

The MD system for simulating flow past a cylinder consisted of 160,000 particles in a square (2D) of side 1500 Å. The particles, under the influence of an acceleration field, flow past a cylinder with thermalizing boundaries. The radius of the cylinder is about 125 Å. The external boundaries are the same as those used in the flow past a plate simulation. That

is, the boundaries parallel to the direction of flow are periodic; the boundaries perpendicular to the direction of flow are modified periodic.

Again, simulations were run for a number of different values of the acceleration field. We show results for one run where the acceleration field was 7.2×10^{13} cm/sec^2. In Fig. 4, the average system velocity is plotted as a function of time (the simulation started with the system at rest). After about 800 psec of simulation time, two counterrotating vortices appear immediately behind the cylinder. These vortices increase in size over the next 700 psec, and then begin separating from the cylinder. The separation process is one in which each vortex in turn detaches from the cylinder and moves downstream. Separation oscillates between the two vortices. The series of streamline contours shown in Fig. 5 graphically demonstrates the oscillating separation phenomena. This behavior repeats itself approximately every 600 psec. The Reynolds number for this final state is somewhere in the range of 30–70 (variations in density and stress prevent a more accurate determination). The Strouhal number is approximately 0.15. It is remarkable that a system with a length scale measured in angstroms and a velocity measured at 30,000 cm/sec shows the same scaling as that seen in macroscopic systems.

6. RAYLEIGH–BENARD CONVECTION

The Rayleigh–Benard problem is perhaps the most studied hydrodynamic instability. It comes about as a result of competition among

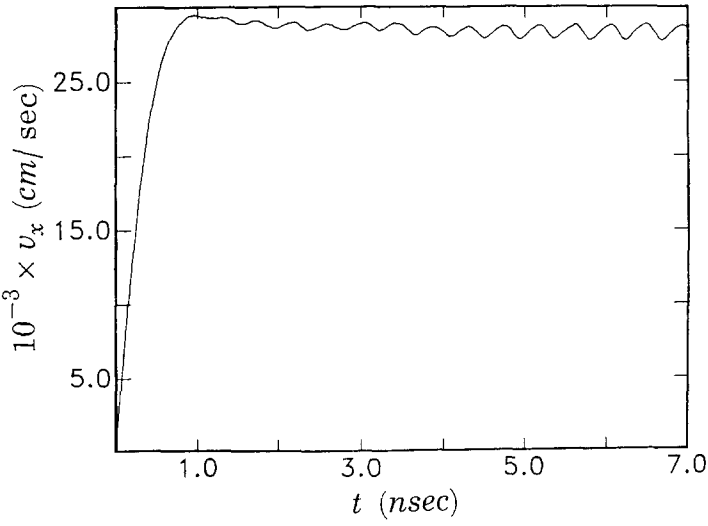

Fig. 4. Velocity as a function of time for flow past a cylinder.

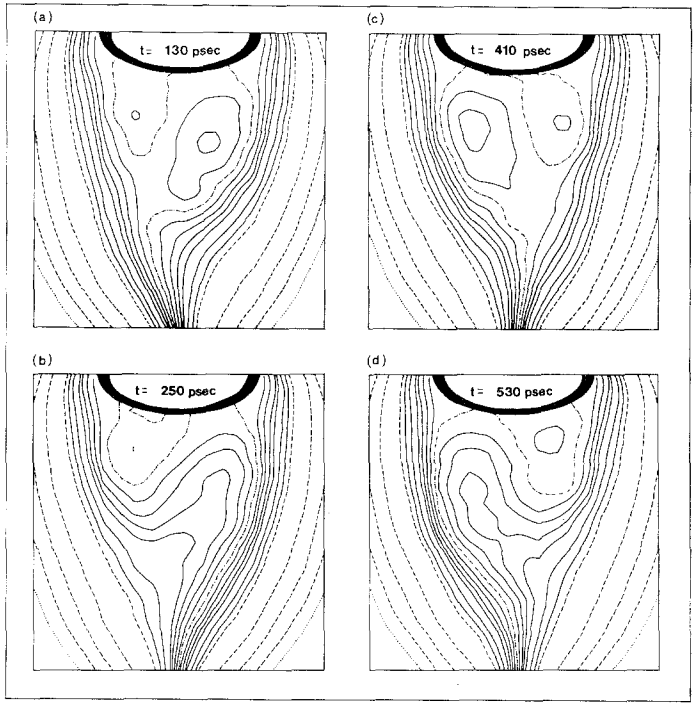

Fig. 5. Streamline contours at (a) $t = 130$ psec, (b) $t = 250$ psec, (c) $t = 410$ psec, and (d) $t = 530$ psec for flow past a cylinder. (—·—) Streamlines are zeros of the stream function representing points of separation or reattachment where in contact with cylinder; (——) streamlines represent steps of 0.1 in the stream function; (— —) streamlines represent steps of 0.5 in the stream function; (...) streamlines represent steps of 1.0 in the stream function.

buoyant forces, thermal dissipation, and viscous drag. A layer of fluid under the influence of a thermal gradient is set up so that the resulting density profile is inverted with respect to the gravitational field. Buoyant forces cause the lighter material to rise; viscous forces present a drag on any motion; thermal dissipation leads to equilibration of the rising material with its surroundings. The competition among these three processes and the resulting behavior in the fluid can be characterized by the dimensionless Rayleigh number, defined as

$$\mathrm{Re} = \frac{\alpha \Delta T g}{\kappa \nu} d^3$$

where α is the compressibility, ΔT is the temperature difference across the fluid layer, g is the magnitude of the gravitational field, κ is the thermal diffusivity, ν is the kinematic viscosity, and d is the depth of the fluid layer.

A linear stability analysis of the hydrodynamic equations for this system shows that the state in which heat is conducted through the layer becomes unstable to a state in which heat is convected through the layer at a critical value of the Rayleigh number R_c dependent on the nature of the top and bottom boundaries ($R_c = 657.5$ for slip boundaries; $R_c = 1707.8$ for no-slip boundaries).[25] At these marginal stability points, convection sets in at a selected wavelength that determines the spatial periodicity in the direction perpendicular to both the thermal gradient and the gravitational field ($\lambda = 2.828d$ for slip boundaries; $\lambda = 2.016d$ for no-slip boundaries). A convection cell, defined over one wavelength, consists of a pair of counter-rotating vortices.

The MD system for simulating this instability consisted of 200,480 particles in a rectangle (2D) of length $L = 3341$ Å and depth $d = 836$ Å (4: 1 aspect ratio). The top and bottom walls are thermalizing boundaries; the side walls are specular boundaries. The bottom wall is maintained at 486.5 K, the top wall at 86.5 K. The magnitude of the gravitational field is used as the control parameter. A rough calculation, using experimental values for the transport coefficients (at $T = 86.5$ K), shows that a gravitation field in the range of 10^{14}–10^{15} cm/sec^2 should yield a Rayleigh number characterizing convective behavior.

The results of simulations of this system proved tantalizing, but not conclusive. In Fig. 6a, we show a contour plot of the stream function, which strongly suggests the existence of a convective state. However, this plot was taken as the system was relaxing to a final steady state (the pressure was changing over time). The pattern remained for a duration of about 500 psec and then disappeared, indicating that the state was a transient. Further, one would expect to see changes in the temperature profile and a jump in the Nusselt number, defined as

$$N = \frac{Q}{k\Delta T}$$

where Q is the heat flux across the layer, if system were in the convective regime. The temperature profile for our system (see Fig. 6b) remained essentially linear; the Nusselt number was not significantly different from unity. Kestemont and Mareschal[26] performed similar simulations with hard spheres and found the same kind of behavior. That is, the convection pattern seemed to appear and disappear over time. Similarly, their temperature profile remained linear across the system (no data were shown for the heat flux). The difficulties in finding the convective regime most probably lie in effects due to the boundary layers such as those discussed in

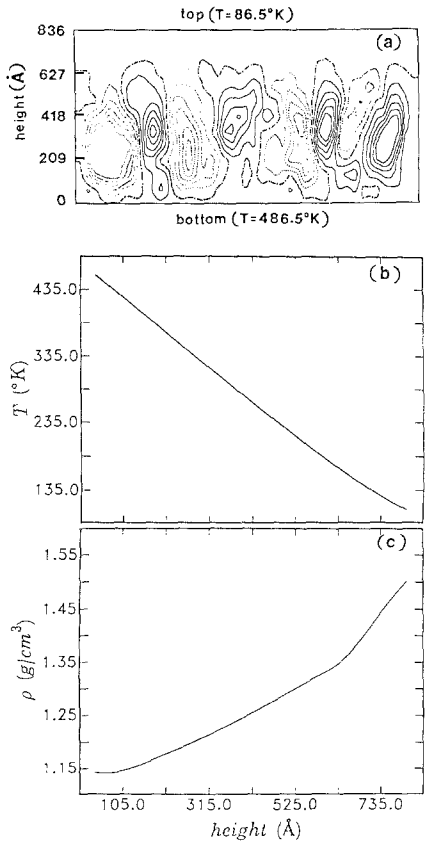

Fig. 6. (a) Streamline contours [(...) streamlines represent clockwise rotation; (——) streamlines represent counterclockwise rotation; (—·—) streamlines represent separate regions of opposite vorticity], (b) temperature profile, and (c) density profile for the Rayleigh–Benard convection.

the above section on channel flow. In the density profile shown in Fig. 6c, we see that the fluid can be divided into three areas: one near the hot boundary, one near the cold boundary, and one in between. The two boundary layers encompass a significant part of the total system. The interplay between the onset of convection and the scale of the boundary layers (or the effective depth of the system, taking account of the boundary layers) could play a major role in determining whether we can or cannot see convection in such small systems.

7. CONCLUSIONS

The feasibility of using molecular dynamics for simulating hydrodynamic phenomena is established. In our simulations and in those done elsewhere, MD systems not only exhibit spatial and temporal structures, they also seem to obey the scaling relations associated with these phenomena in macroscopic theory and experiment. Because of computational intensity, it is very unlikely that the MD simulations will ever completely replace the more traditional methods for solving the Navier–Stokes equations. However, they can play an important role in supplementing these methods in describing macroscopic phenomena and provide microscopic underpinnings of the macroscopic theories. Furthermore, MD can be used to study phenomena where the Navier–Stokes approach is no longer applicable.

ACKNOWLEDGMENTS

We thank Prof. V. Yakhot for discussion on the channel flow problem, Prof. D. Rapaport for discussion on the flow past a cylinder problem, and Prof. M. Malek Mansour for discussion on the Rayleigh–Benard problem.

REFERENCES

1. G. Ciccotti and W. G. Hoover, eds., *Molecular Dynamics Simulations of Statistical Mechanical Systems* (North-Holland, Amsterdam, 1986).
2. D. J. Evans and W. G. Hoover, *Annu. Rev. Fluid Mech.* **18**:243 (1986).
3. W. G. Hoover and W. T. Ashurst, in *Theoretical Chemistry*, Vol. I, H. Eyring and D. Henderson, eds. (Academic Press, New York, 1969).
4. C. Trozzi and G. Cicotti, *Phys. Rev. A* **29**:916 (1984).
5. D. J. Evans, *Phys. Lett. A* **91**:457 (1982).
6. M. J. Gillian and M. Dixon, *J. Phys. C* **16**:869 (1983).
7. M. M. Mansour, A. L. Garcia, G. C. Lie, and E. Clementi, *Phys. Rev. Lett.* **58**:874 (1987).
8. J. J. Erpenbeck, *Physica* **118A**:144 (1983).
9. D. J. Evans, *J. Stat. Phys.* **22**:81 (1980).
10. W. G. Hoover, D. J. Evans, R. B. Hickman, A. J. C. Ladd, W. T. Ashurst, and B. Moran, *Phys. Rev. A* **22**:1690 (1980).
11. T. Naitoh and S. Ono, *J. Chem. Phys.* **70**:4515 (1979).
12. W. T. Ashurst and W. G. Hoover, *Phys. Rev. A* **11**:658 (1975).
13. A. Tennenbaum, G. Cicotti, and R. Gallico, *Phys. Rev. A* **25**:2778 (1982).
14. A. L. Garcia, M. M. Mansour, G. C. Lie, and E. Clementi, *Phys. Rev. A* **36**:4348 (1987).
15. C. W. Gear, *Numerical Initial Value Problems in Ordinary Differential Equations* (Prentice-Hall, Princeton, New Jersey, 1971).
16. L. Hannon, G. C. Lie, and E. Clementi, *Phys. Lett. A* **119**:174 (1986).

17. F. F. Abraham and Y. Singh, *J. Chem. Phys.* **67**:2384 (1977).
18. A. K. Macpherson, Y. P. Carignan, and T. Vladimiroff, *J. Chem. Phys.* **86**:4228 (1987).
19. A. L. Robinson, *Science* **236**:150 (1987).
20. Tosio Miyagi and Takahiro Kamei, *J. Fluid Mech.* **134**:221 (19836).
21. E. Meiburg, *Phys. Fluids* **29**:3107 (1986).
22. L. Hannon, G. C. Lie, and E. Clementi, *J. Sci Comput.* **1**:145 (1986).
23. L. D. Landau and E. M. Lifshitz, *Fluid Mechanics* (Pergamon Press, Oxford, 1982).
24. M. Braza, P. Chassaing, and H. Ha Minh, *J. Fluid Mech.* **165**:79 (1986).
25. S. Chandrasekhar, *Hydrodynamic and Hydromagnetic Stability* (Dover, New York, 1981).
26. E. Kestemont and M. Mareschal, *J. Stat. Phys.* **48**:1187 (1987).